J Supercond Nov Magn (2013) 26:3231–3234
DOI 10.1007/s10948-013-2191-7

ORIGINAL PAPER

Fabrication of Flux Qubit with a Mechanical Degree of Freedom

K. Harrabi

Received: 5 February 2013 / Accepted: 16 March 2013 / Published online: 2 April 2013
© Springer Science+Business Media New York 2013

Abstract We report on the fabrication and characterization of superconducting flux qubit coupled to nanomechanical resonator vibration modes. Anisotropic and isotropic etching processes parameters of plasma created by a reactive ion etching of a CF_4 gas, were optimized to suspend one arm of the qubit. One of the beams was characterized using a magnetomotive detection scheme in the transmission regime. And suspended beams with different length coupled to a superconducting flux qubits were characterized at base temperature by performing spectroscopy measurements.

Keywords Superconductivity · Qubit · Nanomechanical resonator

1 Introduction

Nanomechanical resonators systems (NEMS) were under the scope of many studies in the past years for their promising potential integrations in nanostructures. They have the advantage to be operated at a microwave frequency range, and offer a high quality factor and low power dissipation [1, 2]. In addition, the low mass and small size of NEMS make them excellent candidates for high-precision force, mass, and position detection, with a sensitivity that is ultimately limited only by quantum mechanics [1, 2]. The focus is oriented toward the detection of vibration of flexural modes of nanomechanical resonators near the quantum limit. Recently, many reports deployed sensitive superconducting quantum devices for this detection near the quantum limit [3, 4].

The approach of this experiment is the detection of the vibration mode of beam in the quantum regime using a flux qubit. The quantum regime requires hf_0 to be larger in comparison to $k_B T$, where f_0 is the beam fundamental resonance frequency, h Plank's constant, and T is the temperature. A few approaches have been pursued including the use of a superconducting transmission line resonator [5] or a high-frequency tank circuit [6] capacitively coupled to the beam. In the latter case, the capacitive coupling can be made strong by reducing the gap between the beam and the driving gate [4]. Some theoretical papers propose qubits as quantum-limited detectors for the displacement of nanomechanical resonators with a flexural resonance mode [7], however, with this scheme the resonator was measured in the classical regime so far [3].

For a simple integration of the nanomechanical resonator in a quantum device, we have developed a method to fabricate radio frequency beam resonators doubly clamped made of Al films. This method presents an advantage to be matched with any fabrication process, since most of the fabricated quantum devices based on the Josephson junctions, used Al as a basic material (flux qubit, charge qubit, transmon, quantronium). Moreover, the plasma created by a reactive ion etching (RIE) uses a single gas fluorinated (CF_4) to etch locally the SiO_x as a sacrifice layer. Two successive processes were used, anisotropic and isotropic, where the RF power and the gas pressure were optimized. During the etching process, only a small window including the beam will be exposed to the plasma and the rest of the chip remains protected from the plasma by a resist layer. This may be important to protect the rest of the qubit circuit, which

K. Harrabi (✉)
Physics Department, King Fahd University of Petroleum and Minerals, 31261 Dhahran, Saudi Arabia
e-mail: harrabi@kfupm.edu.sa

K. Harrabi
The Institute of Physical and Chemical Research (RIKEN), Wako, Saitama 351-0198, Japan

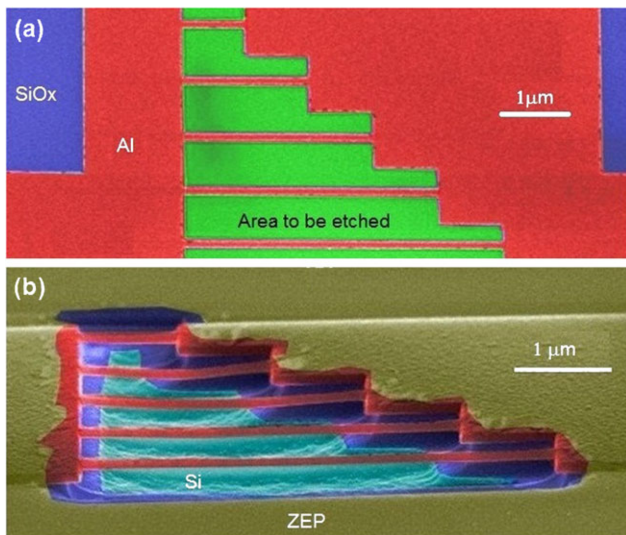

Fig. 1 (**a**) Top view in SEM image of five doubly clamped beams and showing the area to be exposed to CF_4 plasma. (**b**) Side view in SEM image of the doubly clamped beams after they were released by combining anisotropic and isotropic process. Residues of the ZEP resist are visible on the metal surface

may be affected by the aggressive plasma. Beams with different length (0.5–7 µm) and the same width (100 nm) were coupled to qubit with different splitting energy. We have designed nanomechanical resonators having different aspect ratios (see Fig. 1a). The resonance frequency of the fundamental flexural mode of these resonators cover the range from about 30 MHz up to about 750 MHz. The highest frequency should correspond to the quantum regime of the resonator cooled down to below 40 mK. In fact, the resonance frequency as high as 770 MHz was reported for resonators of similar design in [8], so there is no doubt that these high frequencies are achievable in the experiment. However, magnetomotive measurements in this experiment were done on one low-frequency (about 30 MHz) resonator just because of simplicity: lower frequency resonators are more compliant and give stronger response, and are therefore easier to characterize. We fabricated beams using this method, and coupled them to superconducting flux qubits. Few devices were tested at low temperature, and spectroscopy measurements were performed.

2 Beam Patterning in Al Film

The fabrication process starts with the deposition of a Al film through a suspended mask formed by electron-beam lithography and dry etching technique. The fabrication details are as follows. A Si wafer covered by a 300 nm thick layer of SiO_x with the prefabricated 100 nm thick Au contact pads and a coplanar line on top is covered by a trilayer resist structure. The trilayer consists of (from bottom to top) a 400 nm thick copolymer layer, 30 nm thick Ge layer, and a 50 nm thick polymethylmethacrylate (PMMA). After the exposure of the top layer in the electron-beam (EB), writer JEOL JBX-5FE and development in a 3:1 mixture of isopropanol (IPA) and methyl-isobutyl-ketone, the pattern in the PMMA is transferred into Ge layer by reactive ion etching in CF_4. This is followed by the removal of the copolymer and undercut creation using oxygen plasma in an electron cyclotron resonance etching machine. Simultaneously, the top PMMA layer is etched away. Finally, a 60 nm thick Al film is deposited through the mask in the electron-gun evaporator, which is followed by the liftoff process in acetone [9]. Figure 1a shows the Al beams after deposition and the area to be etched.

After the Al beams are deposition, the wafer is spin-coated with the positive resist ZEP520A-7, and baked at 150 °C. The area surrounding the beam was exposed in the EB writer, and then developed in xylene and rinsed in IPA. The developed area form a window though which the SiO_x layer will be subsequently etched away in a CF_4 plasma. We utilized two etching steps: anisotropic process followed by the isotropic process.

The sample is placed inside a chamber of RIE machine (SAMCO-10NR), in which a CF_4 gas was fed in. The plasma is created; the ions are accelerated toward, and react at, the surface of the whole wafer. We used the property of the physical part of reactive ion etching, since the ions have high enough energy, they can remove atoms out of the material to be etched without a noticeable chemical reaction, the SiO_x in our case. Its parameters were optimized by increasing the RF power and setting a low pressure. During this anisotropic process, both ZEP resist and the SiO_x are being etched away, but they differ in the etching rate as shown in the schematic.

After the anisotropic process is accomplished, a SiO_x wall remains not etched and protected by the beam, the latter played a role of a mechanical mask. We used the property of the isotropic etching, which is the non-directional removal of material and targeting the remaining SiO_x wall. Via a chemical process, the power and the pressure were increased and the SiO_x was etched away beneath the beam, the beams were released (Fig. 2b). The remaining ZEP was ashed away using an oxygen plasma. The optimized parameters are for: anisotropic: $P = 200$ W, $p = 10$ Pa and $\Delta t = 1$ min 50 s and isotropic: $P = 240$ W, $p = 240$ Pa and $\Delta t = 15$ min 30 s.

3 Characterization of the Beam

Figure 2a shows a schematic of an experimental setup we used to characterize our beams. The sample was mounted in a dilution refrigerator and cooled down to 30 mK. The NEMS was connected to the network analyzer at room temperature through coaxial cables, and a 3 dB attenuator is

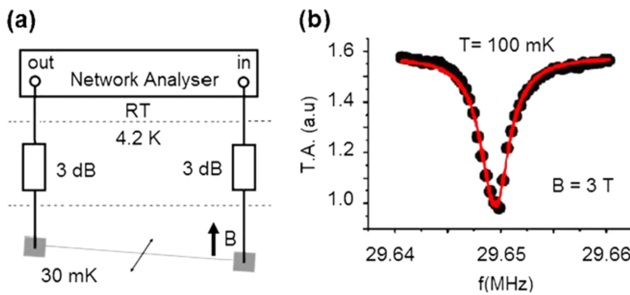

Fig. 2 (**a**) Schematic of the measurement setup used to study the suspended beam; (**b**) The resonance frequency dip of the beam measured at 100 mK in a transverse magnetic field of 3 T. The experimental data was fitted with a Lorentzian function (TA: transmission amplitude) (Color figure online)

mounted in the input and output signals. It was characterized by using a magnetomotive detection scheme in the transmission regime. The alternating current from the output of the network analyzer is fed into the circuit, transverse to the magnetic field applied by a superconducting coil fixed outside the sample package. It generates a Lorentz force ($\vec{F} = i\vec{L} \times \vec{B}$) that drives the beam transverse to its length and to the field direction, in the substrate plane. The applied power in the circuit is kept low to work in the linear regime of the beam. The frequency of the ac signal is swept and on resonance the motion of the beam then generates an electromotive force EMF (V_{emf}) along the length of the beam. V_{emf} is derived from the S_{21} parameter measured by the network analyzer, resulting in a dip in the transmission at the resonant frequency. The resonant frequency of the beam is $f = \frac{w}{L^2}\sqrt{\frac{E}{\rho}}$ [10], where L is the length of the beam, w its width, E and ρ are the Young's modulus, and the density, respectively.

A 4 μm long suspended beam using this technique was measured and characterized. Figure 2b shows a measurement of the resonant frequency of the NEMS at $B = 3$ T and 100 mK. On resonance, the beam dissipates energy producing a deep in the transmitted signal; it is well fitted with a Lorentzian function. The full width half-maximum (FWHM $= \Delta f$) is deduced, the quality factor is given by $Q = f_0/\Delta f$, where f_0 is the resonant frequency at the applied magnetic field. The fundamental limit to the Q of nanomechanical resonators is imposed by several loss mechanisms including, for example, thermoelastic losses, surface losses, and damping caused by two-level fluctuators located in the resonators. The contribution from the former one is negligible: It is emphasized in [11] that thermoelastic damping is a significant source of dissipation for MEMS and NEMS at temperatures around 100 K and above. The origin of thermoelastic damping is well understood as being caused by the nonlinear interaction of the resonators modes with a surrounding bath of thermally-excited elastic modes, or phonons. The origin of the latter two mechanisms is still unclear and deserves further studies. The presence of two-level fluctuators in Al nanomechanical resonators, which were similar to those studied in this work, was reported in [8]. In the magnetomotive method presented in this work, the dominant damping contribution comes from magnetomotive damping, which is proportional to the motional impedance that scales as B^2. Therefore, it dominates in high magnetic fields and produces an overall parabolic dependence of $1/Q$ vs. B.

Since the beam was measured in the normal state, the Q value for $B = 0$ T was obtained by the extrapolation of the magnetic field dependence to zero field. The resonant frequency of the beam was $f = 29.64$ MHz, and the quality factor $Q \sim 1.2 \times 10^4$ [12]. In the absence of tension, the formula of f gives the resonance frequency of 31.85 MHz, which is about 7.5 % higher than the measured value, apparently due to the remaining compressive stress in the beam. The stress is due to the difference in thermal contraction between Al and the SiO_x. Based on previous studies, Al beams made using this technique are similar to those made of single crystal materials, such as Si, AlN, and GaAs. Our beams showed a high quality factor $\sim 10^4$, which is comparable to what was obtained on other beams made of various materials and fabricated by different processes.

4 Superconducting Flux Qubit Coupled to the Mode of the Nanomechanical Resonator

The sample was fabricated using electron-beam lithography (EBL) and shadow evaporation techniques. It was made out of Al, and part of the qubit loop is shared with a microwave line, which is used for the dispersive measurements as a readout device [13]. It was made using a trilayer process, and the suspension process was performed at last step. Many qubits with suspended arms were fabricated and coupled to the same microwave line. Two qubits having suspended beams with different length are shown in Fig. 3. They were designed with different splitting energies and areas.

In this coupling scheme, the qubit's persistent current (I_p) passes through a nanomechanical resonator, which is one part of its arm. And the applied perpendicular bias magnetic field of the qubit generates a Lorentz force in the plane of the beam. Thus, the persistent current induces a Lorentz force with opposite directions for a clockwise and counterclockwise current. The vibration of the beam is modulated by these Lorentz forces. Then the vibration mode of the beam is coupled to the quantum state of the flux qubit. The coupling term is $g = BI_pL\Delta x$ [14], where B is the applied magnetic field, and Δx the displacement of the beam.

Spectroscopy data for 4, 5, and 7 μm beams coupled to a flux qubit is shown in Fig. 4b. The parameters of qubits are, for qubit 1 ($\Delta_1 = 9.6$ GHz, $I_{p1} = 190$ nA), qubit 2 ($\Delta_2 =$

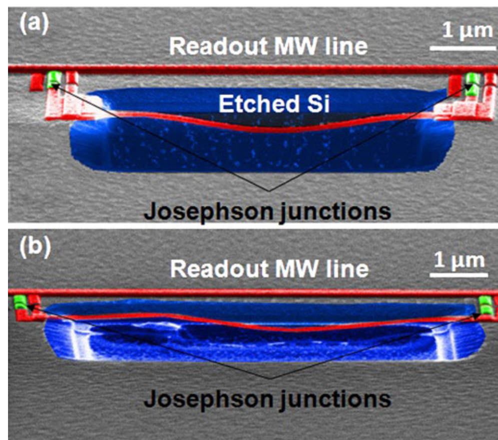

Fig. 3 Side view in SEM of the flux qubit with different angles. (**a**) One arm of the loop is suspended and having 5 µm length and (**b**) with 7 µm (Color figure online)

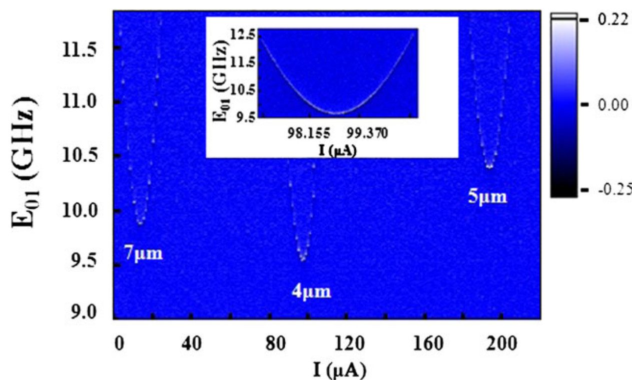

Fig. 4 Spectroscopy measurements: the E_{01}/h vs. applied current of the magnet, three visible qubits with 4, 5, and 7 µm beams designed to be in this range of the applied magnetic field. The *onset* of figure is a detailed spectroscopy measurements of a qubit with 5 µm suspended beam

9.8 GHz, $I_{p2} = 200$ nA), and qubit 3 ($\Delta_3 = 10.4$ GHz, $I_{p3} = 175$ nA). These parameters are very close to the designed ones and similar to the values reported in [15]. However, the vibration mode was not detected for these three qubits. We believe that the main reason for this was the weak resonator-qubit coupling. The coupling term is proportional to the dc magnetic field threading the qubit loop, which due to technical constraints was limited to below 1 mT only. The coupling will be increased ten times by the tenfold increase of the applied dc magnetic field and, therefore, the detection of the vibration will be observable.

5 Conclusion

In conclusion, a combination of anisotropic and isotropic processes in RIE CF_4 plasma was used to couple resonant modes of a nanomechanical resonator to the superconducting flux qubit by partly suspending one arm of the qubit loop. Measured qubits presented the same parameters as designed and were not affected by the suspension of the qubit arm. This technique will be used in the future for the detection of resonant modes of the mechanical resonator.

Acknowledgements This work was supported by the JSPS through its FIRST Program and MEXT Kakenhi “Quantum Cybernetics.” K.H. gratefully acknowledges the support of the King Fahd University of Petroleum and Minerals, Saudi Arabia, under the FT100009 DSR project.

References

1. Ekinci, K.L., Roukes, M.L.: Rev. Sci. Instrum. **76**, 061101 (2005)
2. Schwab, K.C., Roukes, M.L.: Phys. Today **58**, 36 (2005)
3. LaHaye, M.D., Suh, J., Echternach, P.M., Schwab, K.C., Roukes, M.L.: Nature **459**, 960 (2009)
4. Sulkko, J., Sillanpää, M., Häkkinen, P., Lechner, L., Helle, M., Fefferman, A., Parpia, J., Hakonen, P.J.: Nano Lett. **10**, 4884 (2010)
5. Regal, C.A., Teufel, J.D., Lehnert, K.W.: Nat. Phys. **4**, 555 (2008)
6. Sillanpää, M., Sarkar, J., Sulkko, J., Muhonen, J., Hakonen, P.J.: Appl. Phys. Lett. **95**, 011909 (2009)
7. Armour, A.D., Blencowe, M.P., Schwab, K.: Phys. Rev. Lett. **88**, 148301 (2002)
8. Hoehne, F., Pashkin, Yu.A., Astafiev, O., Faoro, L., Ioffe, L.B., Nakamura, Y., Tsai, J.S.: Phys. Rev. B **81**, 184112 (2010)
9. Li, T.F., Pashkin, Yu.A., Astafiev, O., Nakamura, Y., Im, H., Tsai, J.S.: Appl. Phys. Lett. **91**, 033107 (2007)
10. Postma, H.W.Ch., Kozinsky, I., Husain, A., Roukes, M.L.: Appl. Phys. Lett. **86**, 223105 (2005)
11. Lifshitz, R., Roukes, M.L.: Phys. Rev. B **61**, 5600 (2000)
12. Harrabi, K., Pashkin, Yu.A., Astafiev, O.V., Kafanov, S., Li, T.F., Tsai, J.S.: Appl. Phys. A **108**, 7 (2012)
13. Astafiev, O., Zagoskin, A.M., Abdumalikov, A.A. Jr., Pashkin, Yu.A., Yamamoto, T., Inomata, K., Nakamura, Y., Tsai, J.S.: Science **327**, 840 (2010)
14. Xue, F., Wang, Y.D., Sun, C.P., Okamoto, H., Yamaguchi, H., Semba, K.: New J. Phys. **9**, 35 (2007)
15. Yoshihara, F., Harrabi, K., Niskanen, A.O., Nakamura, Y., Tsai, J.S.: Phys. Rev. Lett. **97**, 167001 (2006)